# *Superior high-temperature electrostatic energy storage in flexible dielectric film enabled by metal-coordination crosslinked network*

*Minhao Yang[1, 2, 3*], Shiang Zhao[1], Yanlong Zhao[1], Haoran Sun[1], Huarui Yan[1], Chong Zhang[4], Jiajun Qu[5], Jun Liu[5, *], Bobo Tian[6, *], Zhi-Min Dang[2, *]*

[1] *Institute of Energy Power Innovation, North China Electric Power University, Beijing, 102206, China*

[2] *State Key Laboratory of Power System Operation and Control, Department of Electrical Engineering, Tsinghua University, Beijing, 100084, China*

[3] *State Key Laboratory of Power Transmission Equipment Technology, School of Electrical Engineering, Chongqing University, Chongqing, 400044, China*

[4] *State Key Laboratory of Advanced Power Transmission Technology, Institute of New Electrical Materials, China Electric Power Research Institute Co., Ltd., Beijing, 102209, China*

[5] *State Key Laboratory of Organic-Inorganic Composites, Beijing University of Chemical Technology, Beijing, 100029, China*

[6] *Key Laboratory of Polar Materials and Devices, Ministry of Education, Shanghai Center of Brain-inspired Intelligent Materials and Devices, Department of Electronics, East China Normal University, Shanghai, 200241, China*

***Correspondence and requests for materials should be addressed to*** *minhao.yang@ncepu.edu.cn (Prof. M. Yang); dangzm@tsinghua.edu.cn (Prof. Z. M. Dang); bbtian@ee.ecnu.edu.cn (Prof. B. Tian); liujun@mail.buct.edu.cn (Prof. J. Liu)*

## 1. Weibull distribution of breakdown strength

Breakdown strength results were analyzed using a two-parameter Weibull statistic described as

$$P(E) = 1-exp\left(-(E/\alpha)^{\beta}\right)$$

Where $P(E)$ is the cumulative probability of breakdown failure, $E$ is the applied electric field, $\beta$ is the scale parameter, which is the breakdown strength at a cumulative failure probability of 63.2%. The shape parameter $\alpha$ is the slope of the fitted Weibull curve, which represents the scattering degree of the experiment results[1,2].

## 2. Hopping conduction mechanism:

The hopping conduction depicts the transport of charge carriers within polymer dielectrics. The thermally excited charge carriers can escape from their trap site to another via a tunneling effect.

$$J = 2qdnv \times exp(-\frac{E_a}{kT}) \times sinh(\frac{qdE}{2kT})$$

Where $d$ is the average hopping distance between adjacent trap sites, $n$ is the electron concentration in the dielectric, $\nu$ is the thermal vibration frequency of the trapped electron, and $E_\alpha$ is the activation energy, $E$ is the applied electric field, $q$ is the electron charge, $k$ is the Boltzmann constant and $T$ is the temperature, respectively. A shorter hopping distance usually indicates a deep trap in the dielectrics[3].

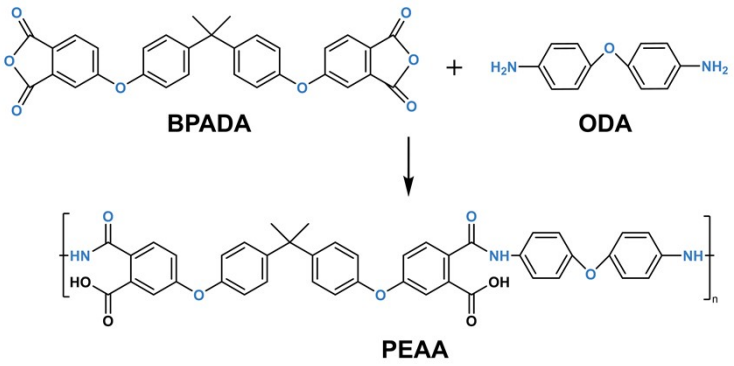


**Figure S1.** The chemical structure of PEAA with abundant pendant carboxyl groups.

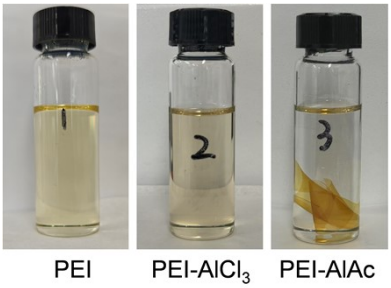


**Figure S2.** Swelling of pristine PEI, PEI-$AlCl_3$ and PEI-AlAc composite films in NMP.

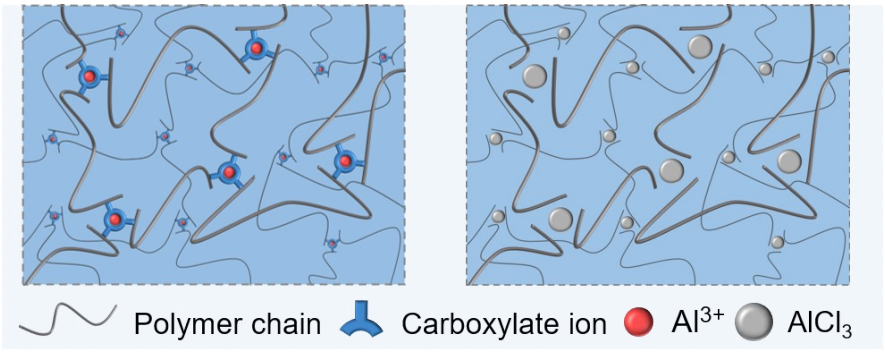


**Figure S3.** Schematic illustration of the structures of PEI-AlAc and PEI-$AlCl_3$ composites.

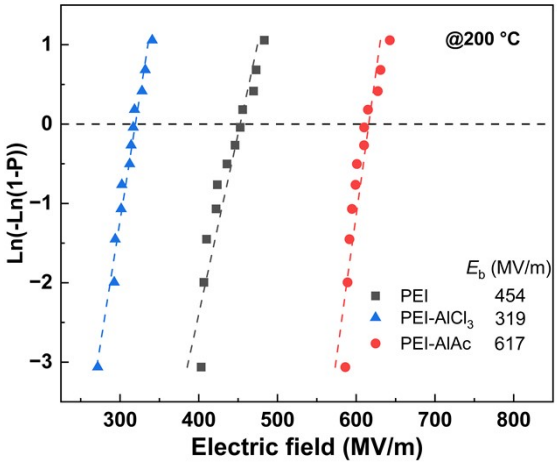


**Figure S4.** Comparison of the breakdown strength of PEI-AlAc and PEI-$AlCl_3$ composites at 200 °C.

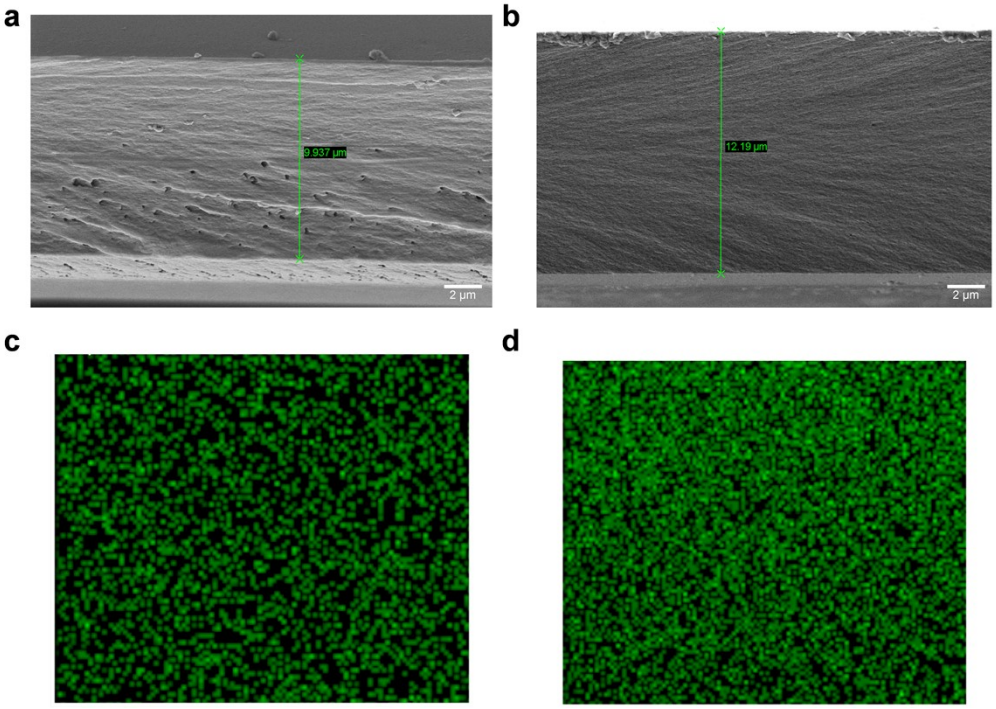


**Figure S5.** SEM images of the fracture surfaces of a) pristine PEI and b) PEI-AlAc composite films; EDS mapping of the Al element on the surfaces of c) pristine PEI and d) PEI-AlAc composite films.

**Table S1.** The statistical concentration of the Al element from EDS mapping of pristine PEI and PEI-AlAc composite films.

| Element | PEI | PEI-AlAc |
|---|---|---|
| Al | 0.03 | 4.13 |

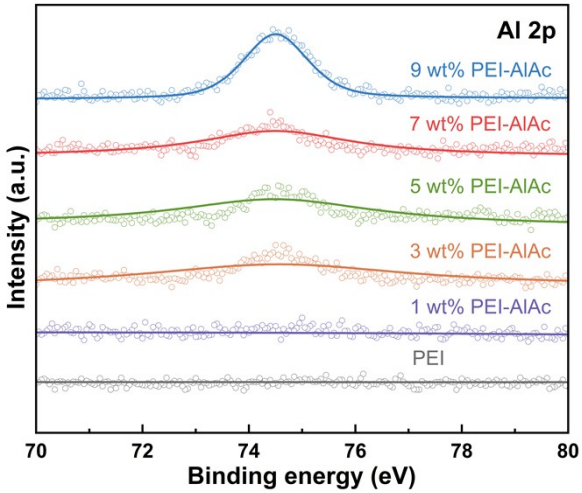


**Figure S6.** XPS Al2p spectrum of pristine PEI and PEI-AlAc composites.

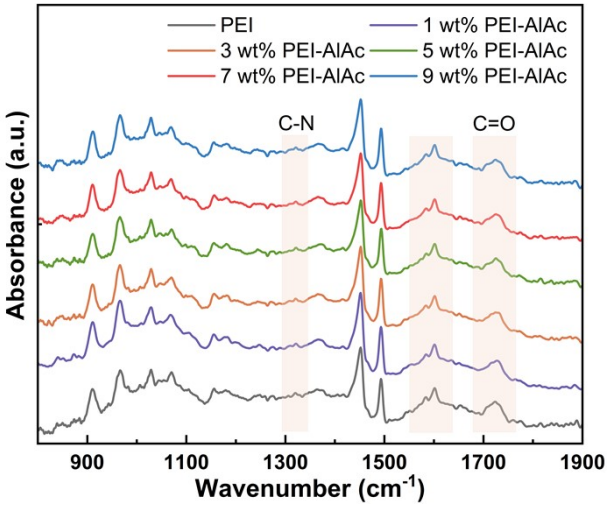


**Figure S7.** FT-IR curves of pristine PEI and PEI-AlAc composites.

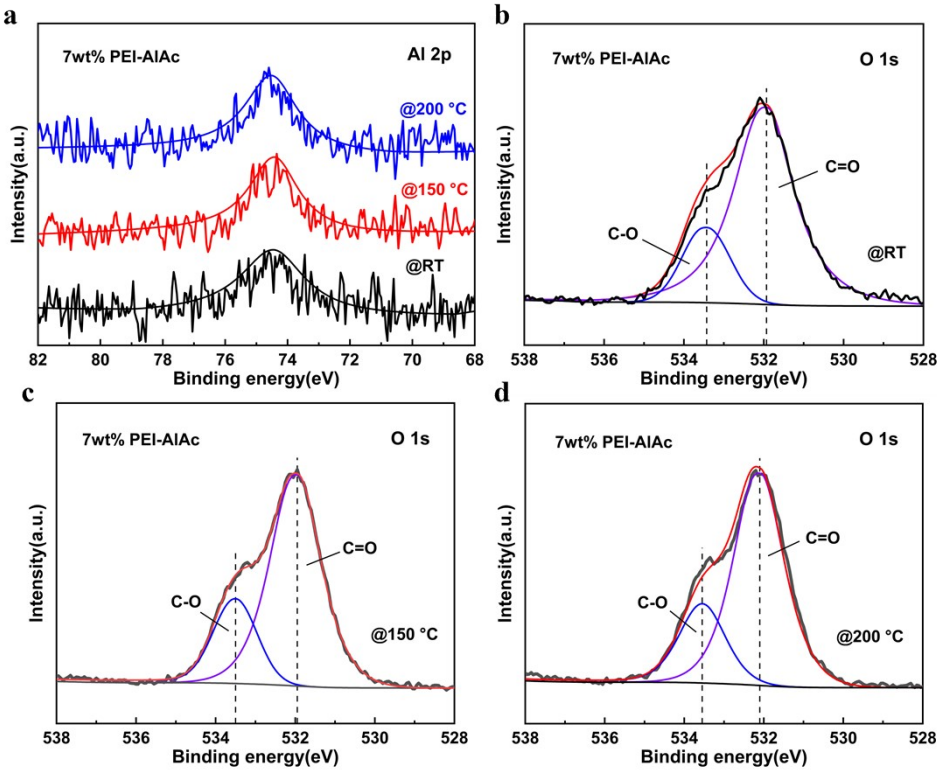


**Figure S8.** In-situ XPS spectra of PEI-AlAc composite at various temperatures.

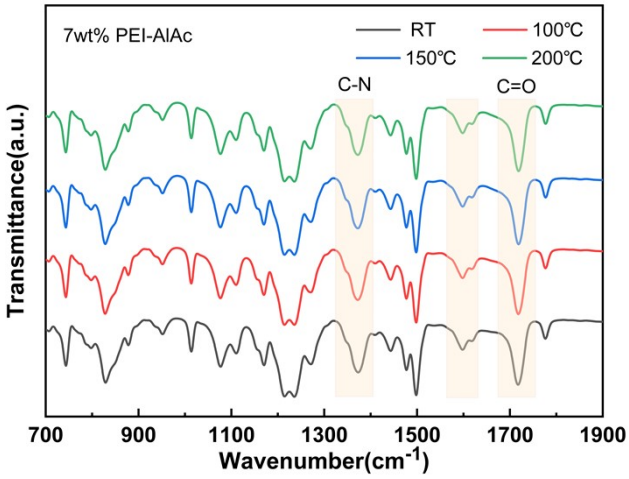


**Figure S9.** In-situ FT-IR curves of PEI-AlAc composite at various temperatures.


**Figure S10.** Swelling of pristine PEI and PEI-AlAc composite films in NMP.

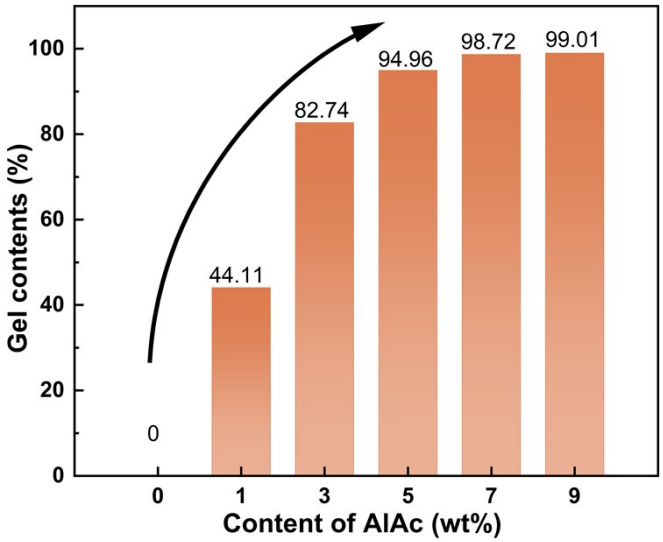


**Figure S11.** Gel contents of pristine PEI and PEI-AlAc composite films.

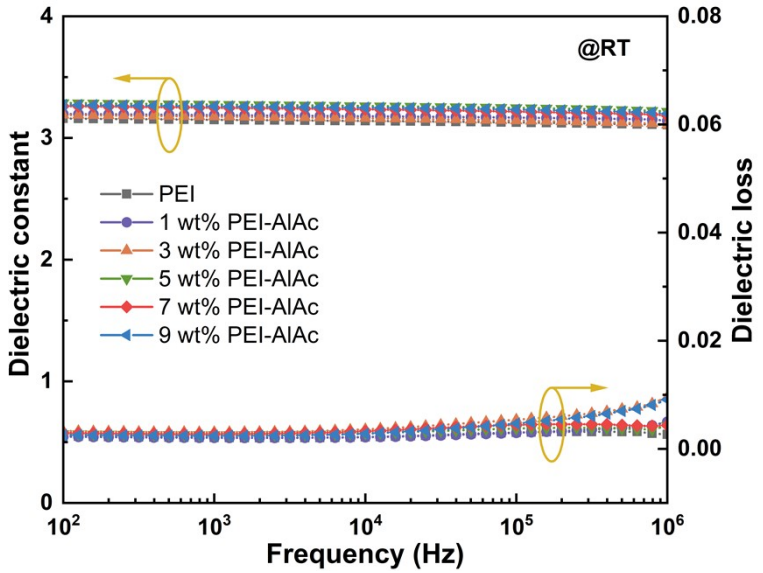


**Figure S12.** Frequency dependence of the dielectric constant and loss of pristine PEI and PEI-AlAc composite films at room temperature (RT).

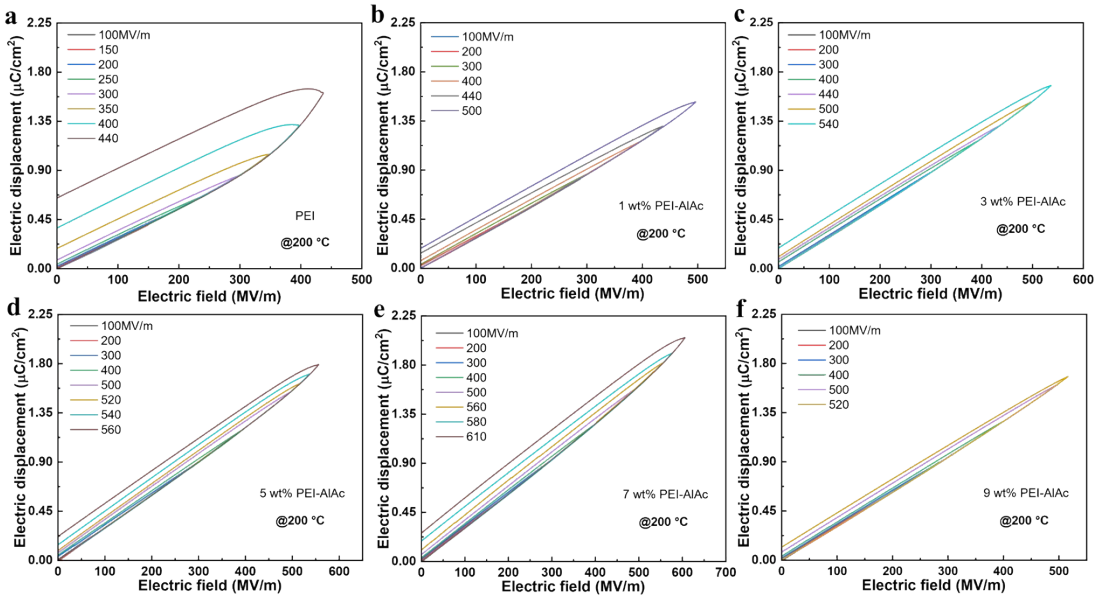


**Figure S13.** Unipolar *D-E* loops of pristine PEI and PEI-AlAc composite films as a function of electric field at 200 ℃.

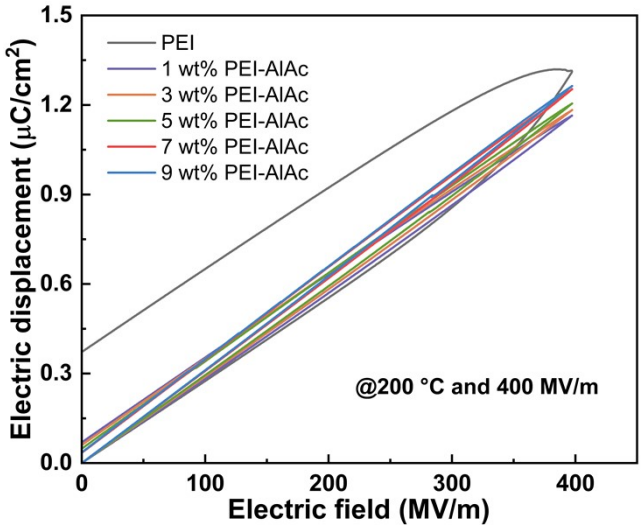


**Figure S14.** Comparison of unipolar *D-E* loops of pristine PEI and PEI-AlAc composite films at 200 ℃ and 400 MV/m.

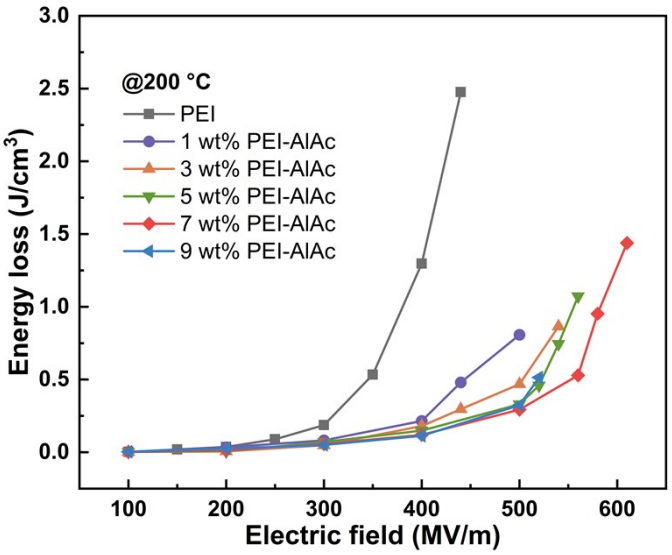


**Figure S15.** Energy losses of pristine PEI and PEI-AlAc composite films as a function of electric field at 200 ℃.

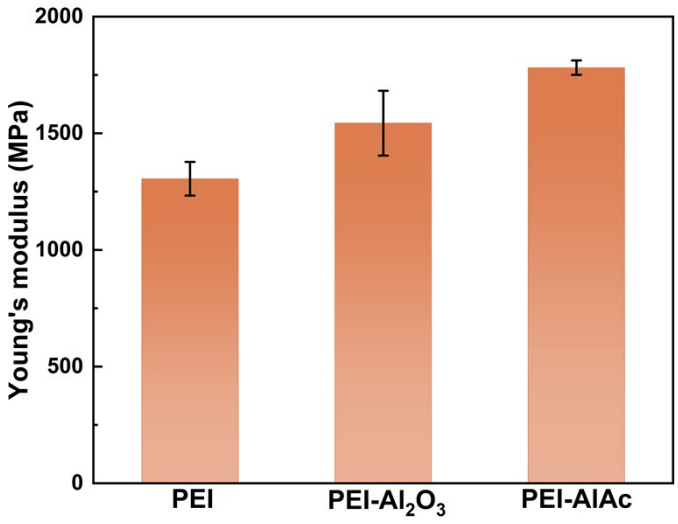


**Figure S16.** Comparison of Young's modulus of pristine PEI, PEI-$Al_2O_3$ and PEI-AlAc composite films calculated from stress-strain curve.

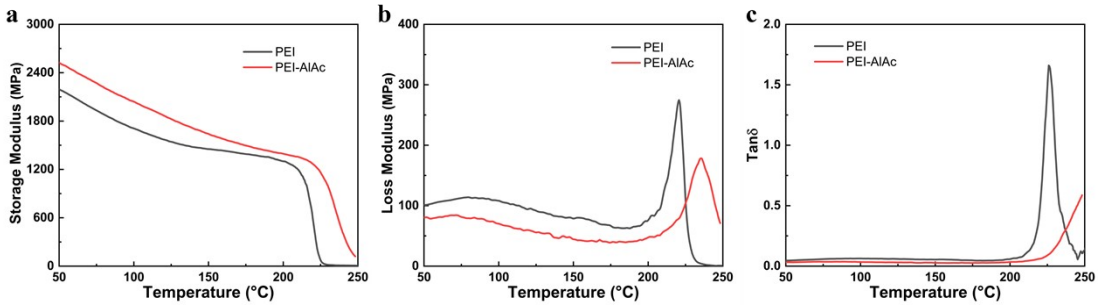


**Figure S17.** DMA curves of pristine PEI and PEI-AlAc composite.

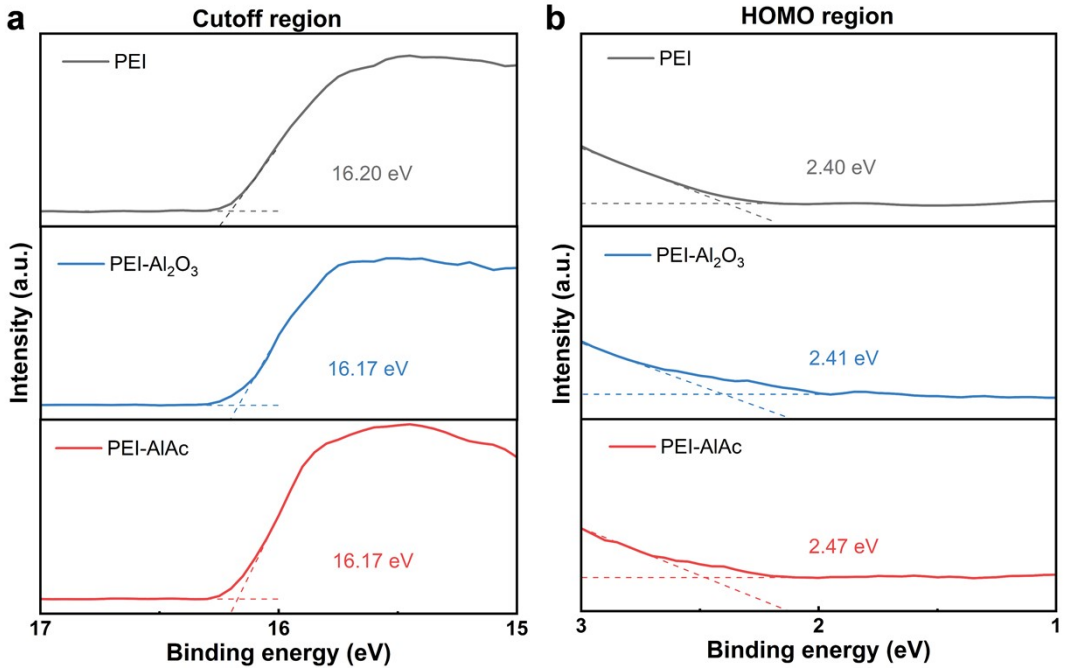


**Figure S18.** UPS spectra of the a) secondary electron cutoff region and b) HOMO region of pristine PEI, PEI-$Al_2O_3$ and PEI-AlAc composite films.

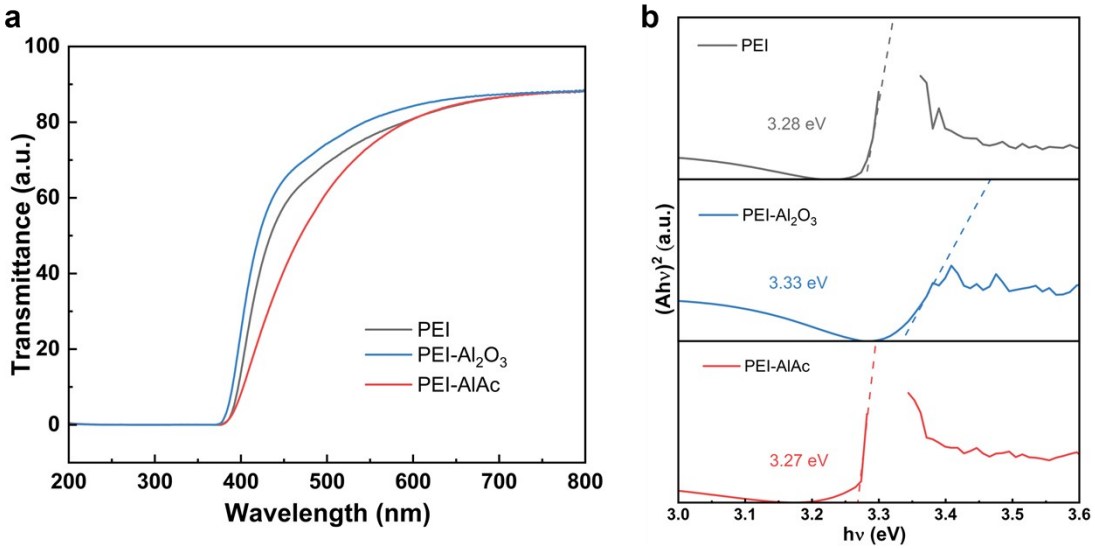


**Figure S19.** a) UV-vis spectra of pristine PEI, PEI-$Al_2O_3$ and PEI-AlAc composite films. b) The optical bandgap calculated from the corresponding UV-vis spectra.

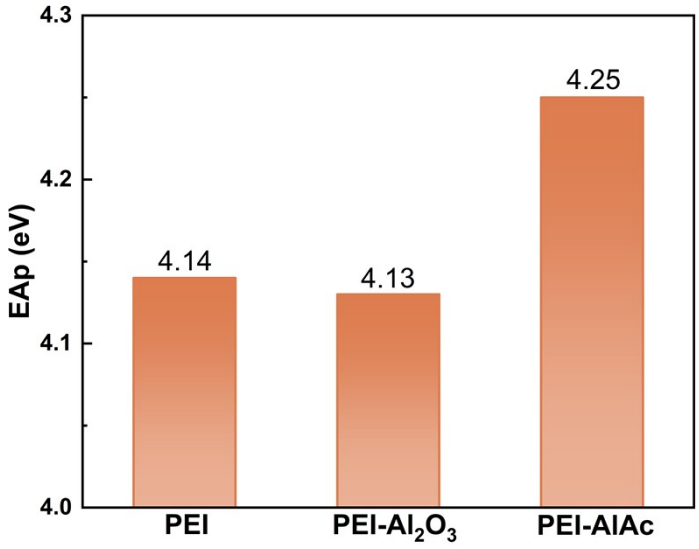


**Figure S20.** The comparison of electron affinity ($EA_p$) for pristine PEI, PEI-$Al_2O_3$ and PEI-AlAc composite films calculated from UPS and UV-vis spectra. The ionization potential (IP) can be calculated by $IP = hv-(E_{cutoff}-E_{homo})$. From this, the position of HOMO level can be determined through the IP value. With the bandgap values from the UV-vis spectra, the position of the LUMO level can be further deduced. The calculated $EA_p$ are 4.14 eV for pristine PEI, 4.13 eV for PEI-$Al_2O_3$ and 4.25 eV for PEI-AlAc, respectively.

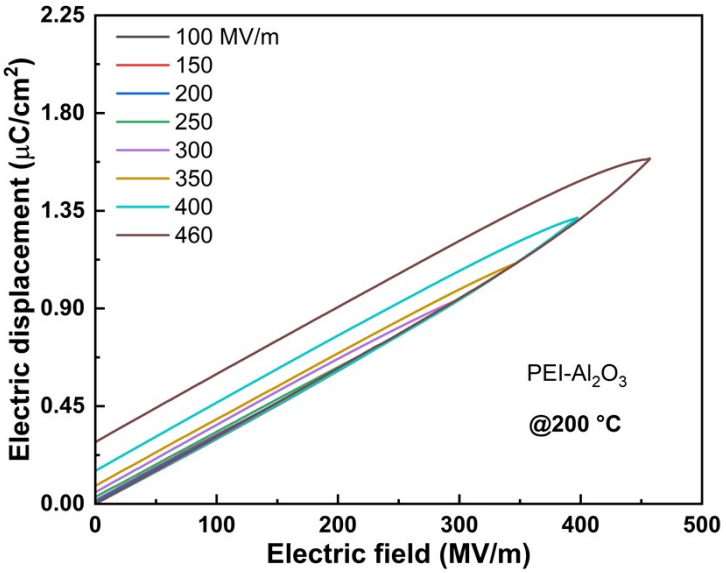


**Figure S21.** Unipolar *D-E* loops of PEI-$Al_2O_3$ composite film at 200 ℃.

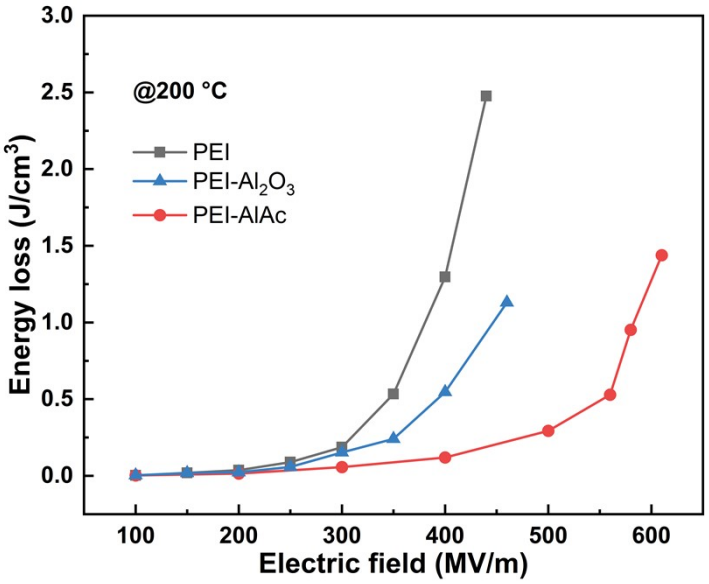


**Figure S22.** Energy losses of pristine PEI, PEI-$Al_2O_3$ and PEI-AlAc composite films at 200 ℃.

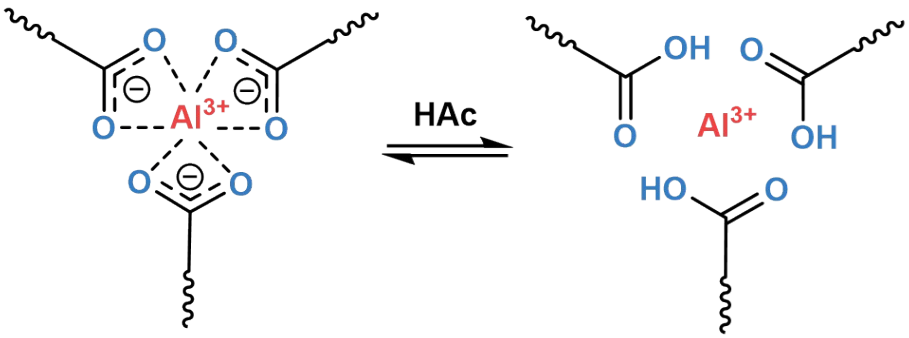


**Figure S23.** Schematic illustration of the dissociation mechanism of the coordinatively crosslinked network via adding or removing the acetic acid.

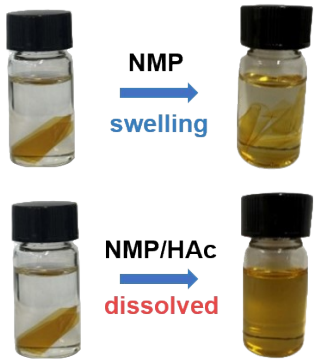


**Figure S24.** Swelling and dissolution of PEI-AlAc composite film under different conditions.

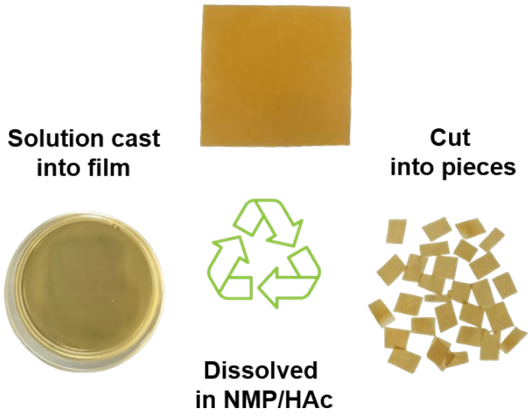


**Figure S25.** The closed-loop recyclability of PEI-AlAc composite film.

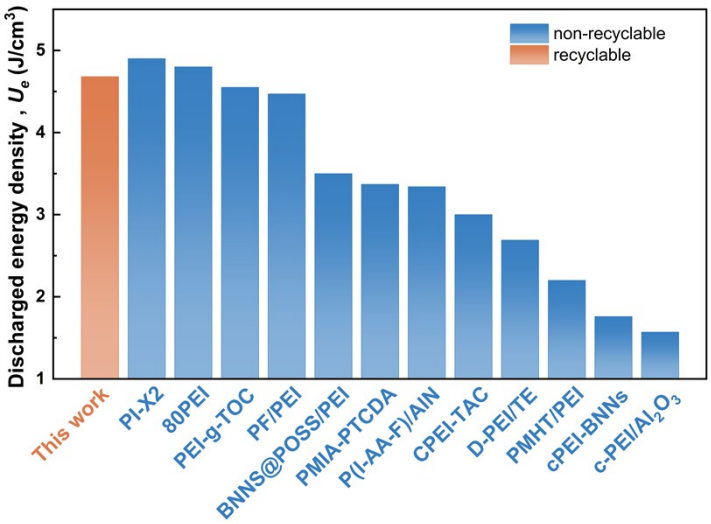


**Figure S26.** Comparison of the recyclability of the sample reported in this work with other typical crosslinked polymer dielectric films exhibiting superior electrostatic energy storage performance at 200 °C[4-15].

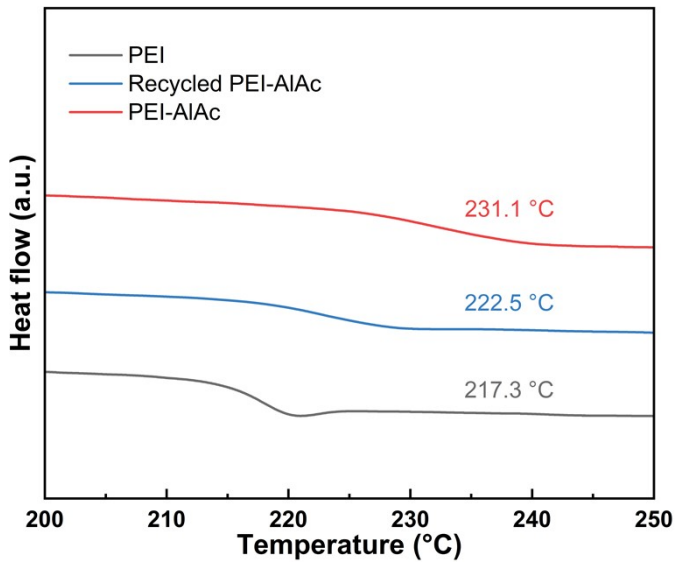


**Figure S27.** DSC curves of pristine PEI, original and recycled PEI-AlAc composite films.

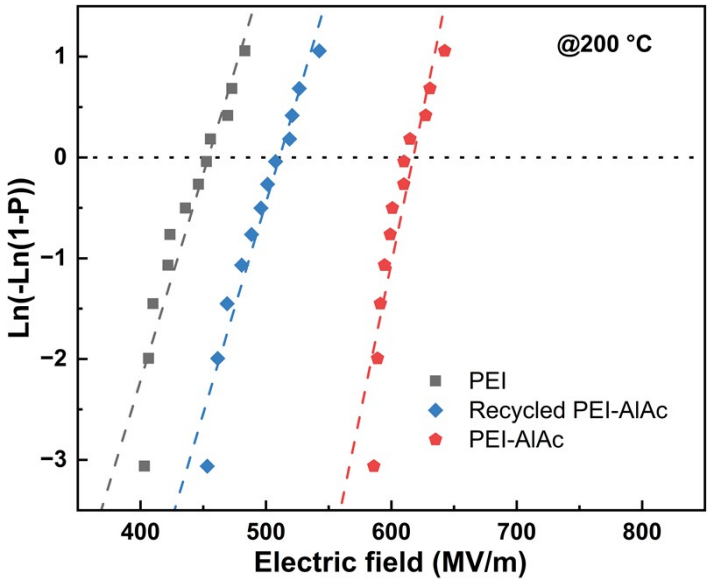


**Figure S28.** Weibull distribution of the breakdown strength of pristine PEI, original and recycled PEI-AlAc composite films at 200 ℃.

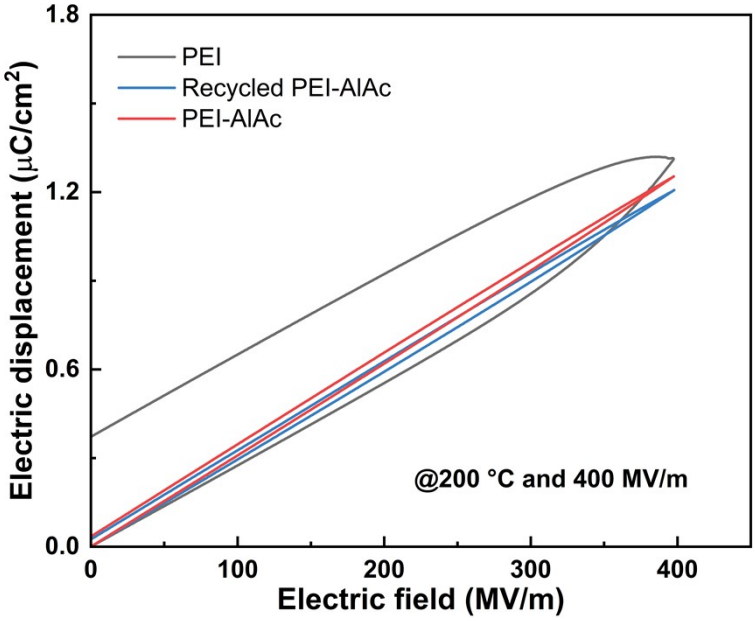


**Figure S29.** Unipolar *D-E* loops of pristine PEI, original and recycled PEI-AlAc composite films at 200 ℃ and 400 MV/m.

## References


1 M. Yang, Y. Zhao, Z. Wang, H. Yan, Z. Liu, Q. Li and Z.-M. Dang, *Energy Environ. Sci.*, 2024, **17**, 1592-1602.

2 M. Yang, Z. Wang, Y. Zhao, Z. Liu, H. Pang and Z.-M. Dang, *Adv Mater.*, 2024, **36**, 2309640.

3 F.-C. Chiu, *Advances in Materials Science and Engineering.*, 2014.

4 W. Zhang, D. Ai, S. Fan, R. Yang, X. Du, X. Yang, F. Lv, Y. Liu, Y. Cheng and X. Yu, Energy Storage Mater., 2025, 77, 104180.

5 S. Zhao, W. Peng, L. Zhou, S. Dai, W. Ren, E. Xu, Y. Xiao, M. Zhang, M. Huang, Y. Shen and C.-W. Nan, Nat. Commun., 2025, 16, 769.

6 Y. Zhou, Z. Zhang, Q. Tang, X. Ma and X. Hou, Mater. Horiz., 2024, 11, 4348-4358.

7 Z. Ran, M. Yang, R. Wang, J. Li, M. Li, L. Meng, Y. Liu, J. Hu, J. He and Q. Li, *Energy Storage Mater.*, 2025, **74**, 103952.

8 L. Zhu, Y. Zhang, W. Xu, X. Zhu, S. Niu, Y. Zhang and Z. Jiang, *Compos Sci Technol.*, 2022, **223**, 109421.

9 Z. Liu, T. Wang, L. Zhu, Z. Jiang and Y. Zhang, *Compos.-A: Appl. Sci. Manuf.***,** 2023, **175**, 107829.

10 D. Hu, H. Luo, Y. Liu, F. Wang, B. Peng, X. Li, H. Wang, G. He and D. Zhang, *Chem. Eng. J.***,** 2024, **498**, 155398.

11 F. Wang, H. Wang, X. Shi, C. Diao, C. Li, W. Li, X. Li, H. Zheng, H. Huang and X. Li, *Chem. Eng. J.*, 2024, **485**, 149972.

12 Y. Wei, L. Yang, C. Wang, Z. Zhu, Y. Dai, H. Qin and C. Xiong, *Chem. Eng. J.*, 2025, **507**, 160793.

13 C. Yan, Y. Wan, H. Long, H. Luo, X. Liu, H. Luo and S. Chen, *Adv. Funct. Mater.*, 2024, **34**, 2312238.

14 X. Dong, Y. Wang, Y. Cao, N. Li, J. Fu, Y. Wang, J. Yu and Z. Hu, *Chem. Eng. J.*, 2024, **500**, 157312.

15 Y. Wan, P. Hu, B. Sun, S. Shen, H. Luo, S. Zhang, D. Zhang, C.-W. Nan and Y. Shen, *Adv. Funct. Mater.*, 2025, **35**, 2506635.